# Analysis of Three-Phase Induction Motor Speed Performance with Load Torque Changes Using Inverter Space Vector Pulse Width Modulation (SVPWM) Control


**Setiyono and Bambang Dwinanto**

**Abstract** This paper presents an analysis of the Space Vector Pulse Width Modulation method which is applied to an inverter for controlling asynchronous alternating current motors or three-phase induction motors through modeling simulations using Simulink MATLAB tools. Induction motors have complex rotational speed control characteristics. Its performance is influenced by several things, including the number of poles, and the frequency setting of the input voltage. To get a wide frequency setting, generally an inverter switch is use which is regulated by controlling the switch gate trigger pulse. This modeling is also used to determine the control pattern of the inverter switch trigger, the characteristics of the voltage curve, torque current, and speed of a three-phase induction motor. This study is also expected to help researchers in solving problems related to the Space Vector Pulse Width Modulation programming algorithm more concisely and easily because the inverter trigger pattern can be directly implemented into electronic control programming. The simulation results show that the induction motor can work on load changes with small torque ripples, stator, and rotor currents with small ripples and is followed by a linear rotational speed setting.

**Keyword** Space vector pulse width modulation · Inverter · Three-phase induction motor

## 1 Introduction

Induction machines as electric power equipment are widely used in various fields, including industry, transportation, offices, and households. Besides having the advantages offered, this machine also has a weakness in setting the rotational speed. The rotational speed of an induction motor can be controlled in two ways, namely direct and indirect starting. Starting directly is done by connecting the motor to the grid voltage. This method has the disadvantage of causing power losses when the motor

Setiyono (✉) · B. Dwinanto
Department of Electrical Engineering, Gunadarma University, Jakarta, Indonesia
e-mail: setiyono@staff.gunadarma.ac.id



T. Triwiyanto et al. (eds.), *Proceeding of the 3rd International Conference on Electronics, Biomedical Engineering, and Health Informatics*, Lecture Notes in Electrical Engineering 1008, https://doi.org/10.1007/978-981-99-0248-4_4

is initially connected to a power source, because at that time the motor draws a very large starting current. The starting method is indirectly by adjusting the supply voltage, input current, stator field flux, and frequency using an electronic device known as a Variable Speed Drive (VSD), especially Inverter [1] [2]. The use of VSD in induction motors has an effect on the improvement of torque, speed, and current drawn by the motor. The study begins with modeling the character control of speed, rotor current, and motor torque [3–7]. Ahmed J. Ali1 modeled the transient regulation approach of a cage-rotor induction motor based on the winding function (WFA) which assumes the MMF coupling between the rotor and stator is sinusoidal and non-sinusoidal. The result is that the second model approach is better [4]. Babak Kiani in his paper writes a Limited Set Model Predictive Direct Torque control method (FS—MPDTC) to reduce torque and flux ripples, by implementing two or more Space Vector Pulse Modulation (SVPWM) voltage vectors [8]. Yassine Zahraoui said space vector modulation is a very appropriate solution to reduce high ripple levels regardless of its complexity [9]. Mihoub Youcef implemented RST and adaptive fuzzy controller (AFC) to increase variable speed Induction motor drive control system [10]. Arkan A. Kadum presents a new adaptive hysteresis band control approach used in direct torque control (DTC) of induction motor drive (IM) with a switching pattern for PWM signal generation; the simulation results under different operating conditions over a wide speed range show the validity, effectiveness, and feasibility of the proposed design [11]. Several other researchers developed induction motor drives with space vector control to obtain lower torque ripple and wider speed regulation [12–19]. Control with VSD is generally done by setting the ignition pattern of the inverter switch using switch control or vector control. Switch ignition settings with vector control have advantages such as more efficient use of energy, and produce a wide rotational speed setting. This study describes a study of induction motor control testing on various changes in load torque using the Space Vector Pulse Width Modulation method to see the character of the stator current, rotor current, and speed of a three-phase induction motor through modeling using the Simulink MATLAB tool. Previous researchers used a lot of Sinusoidal Pulse Width Modulation (SPWM) control method, but in the article the method of generating a gate ignition signal using the Space Vector Modulation (SVPWM) method has a smaller harmonic distortion and a higher output voltage than the SPWM method. The simulation results show that the design of the induction motor speed regulation using SVPWM can work well and is able to operate at changes in load torque. This design can be a technological contribution and a reference for advanced researchers to be implemented into electronic circuits.

## 2 Space Vector Concept

The representation of the time function of a balanced three-phase system of a voltage and current can be shown in Eq. (1):

$$v_a + v_b + v_c = 0 \tag{1}$$

The magnitude and direction of the vector $[v_a 00]^T$ of a three-phase system is placed along the coordinates of the d-axis; the vector $[0v_b0]^T$ is shifted by $120^0$ and the vector $[00v_c0]^T$ is shifted by $240^0$. Figure 1 is an illustration of this vector in imaginary coordinates d-q.

$$\alpha = tg^{-1}\left(\frac{V_d}{V_q}\right) = \omega = 2\pi f \tag{2}$$

where $f$ = fundamental frequency for Eq. (2).

If $v_a$, $v_b$, $v_c$ is specified as a reference, the vector $v_{ref}$ can be determined by Eq. (3):

$$v_{ref} = \frac{2}{3}\left[v_a + v_b e^{j(2/3)\pi} + v_c e^{-j(2/3)\pi}\right] \tag{3}$$

The vector $v_{ref}$ (three-dimensional space) is then transformed into a two-dimensional d-q space base system into an algebra for the sum of real elements and imaginary elements in Eq. (4):

$$\begin{bmatrix} v_d \\ v_q \end{bmatrix} = \frac{2}{3}\begin{bmatrix} 1 & \frac{-1}{2} & \frac{-1}{2} \\ 0 & \frac{\sqrt{3}}{2} & \frac{-\sqrt{3}}{2} \end{bmatrix}\begin{bmatrix} v_a \\ v_b \\ v_c \end{bmatrix} \tag{4}$$

The next step is the transformation of the d-q coordinate space to the $\alpha - \beta$ coordinates obtained by Eq. (5):

$$\begin{bmatrix} v_\alpha \\ v_\beta \end{bmatrix} = \begin{bmatrix} \cos(\omega t) & \cos\left(\frac{\pi}{2} + \omega t\right) \\ \sin(\omega t) & \sin\left(\frac{\pi}{2} + \omega t\right) \end{bmatrix}\begin{bmatrix} v_d \\ v_q \end{bmatrix} = \begin{bmatrix} \cos(\omega t) & -\sin(\omega t) \\ \sin(\omega t) & \cos(\omega t) \end{bmatrix}\begin{bmatrix} v_d \\ v_q \end{bmatrix} \tag{5}$$

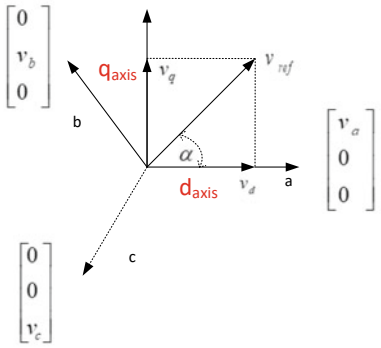


**Fig. 1** Placement of the Vector of a three-phase to d-q Coordinate

If $v_a$, $v_b$, $v_c$ is a three-phase voltage-balanced system with a maximum value of $V_m$, then the vector $v(t)$ can be denoted by Eq. (6):

$$v(t) = V_m e^{j\omega t} \tag{6}$$

Thus, $v(t)$ is a vector with a maximum amplitude of $V_m$ rotating at a constant angular velocity of $\omega$ rad/sec.

## 2.1 Eight Vector Switching Inverter Combinations in Space Vector Pulse Modulation (SVPWM)

The performance of the three-phase inverter switch can be grouped into eight states. Switches a, b, and c have complementary switch pairs a', b', and c' where when switch a is connected or ON then the complementary switch pair a' is open or OFF. Likewise, switch b and switch c work in reverse with their complementary switches b' and c'.

Figure 2 describes a three-phase inverter having eight switching conditions that can be formed in eight binary compositions from 000 to 111. Each composition is denoted by $V_0$, $V_1$, $V_2$, $V_3$, $V_4$, $V_5$, $V_6$, and $V_7$ hereinafter referred to as vector switching. $V_1$, $V_2$, $V_3$, $V_4$, $V_5$, and $V_6$ are called non-zero vectors because they produce an output voltage that is not equal to zero, while $V_0$ and $V_7$ are called zero vectors where this vector produces an output voltage equal to zero.

Figure 3 shows 6 vectors mapped to six sectors (sectors 1 to 6) in a position around the central point forming a hexagonal shape while two vectors are mapped to the center point (origin) [9, 20–22]. Each sector has a vector angular distance of $60^0$. In one rotation on the complex coordinate plane d-q, $V_{ref}$ will pass through the six non-zero vectors and zero vectors. The inverter output voltage is also affected by the SVPWM modulation index. Selection of the right modulation index will assist in the production of the rated voltage. If the modulation index is less, the pulse duration on time will be less and therefore, the device conduction time will also be less, so the inverter output voltage is reduced [23, 24].

Table 1 shows the state of the output voltage ($V_0$–$V_7$) at various switch conditions for each sector.

## 2.2 Time Calculation and Gate Trigger Pattern

The trigger of the inverter switch gate with the SVPWM method is the most important part of this research. Figure 4 explains the basis for calculating the trigger timing of the inverter gate switch based on vector analysis in sector 1. $V_{ref}$ is the resultant of the length of vector $V_A$ and vector $V_B$, and can be represented by Eq. (7):

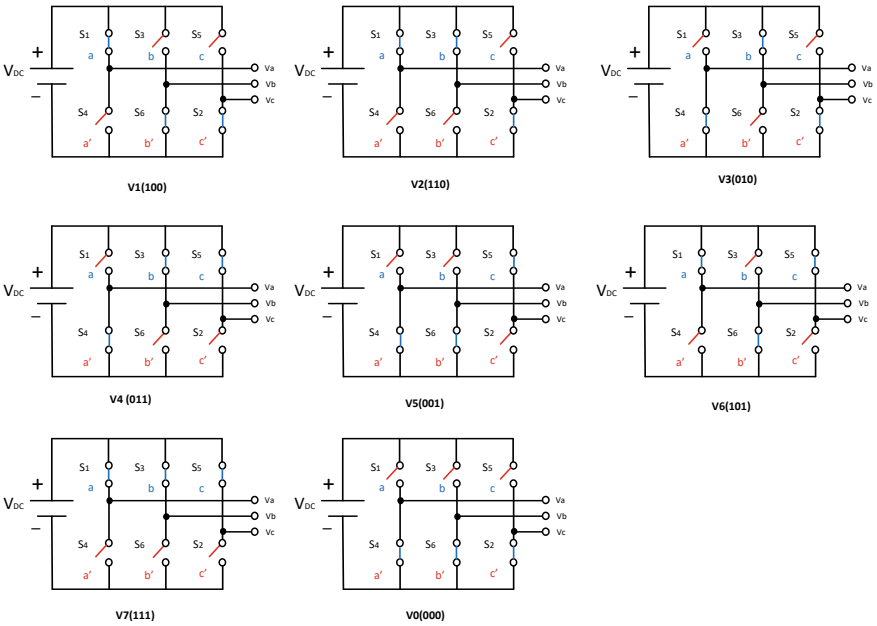


**Fig. 2** Eight combinations of inverter switch conditions

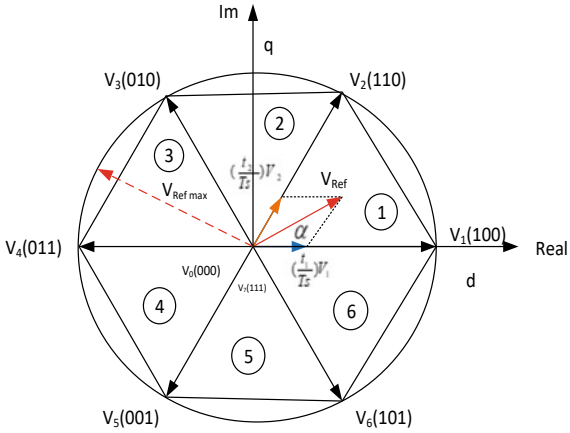


**Fig. 3** The position of each vector on the coordinate plane of two-dimensional space, d-q

$$V_{\text{ref}} = V_{\text{A}} + V_{\text{B}} \tag{7}$$

In each sector, the value of is always in the interval $0 \leq \alpha \leq \frac{\pi}{3}$. The voltage $V_{\text{ref}}$ in sector 1 is of angle $60^0$, the value $V_{\text{A}} = V_1$, $V_{\text{B}} = V_2$, then the voltage $V_{\text{ref}}$ in sector

**Table 1** Inverter output voltage in vector switching state

| Voltage vectors | Sector | Switching vector | | | Line to neutral voltage | | | Line-to-line voltage | | |
|---|---|---|---|---|---|---|---|---|---|---|
| | | a | b | c | $V_{an}$ | $V_{bn}$ | $V_{cn}$ | $V_{ab}$ | $V_{bc}$ | $V_{ac}$ |
| $V_0$ | 0 (origin) | 0 | 0 | 0 | 0 | 0 | 0 | 0 | 0 | 0 |
| $V_1$ | 1 | 1 | 0 | 0 | 2/3 | – 1/3 | – 1/3 | 1 | 0 | – 1 |
| $V_2$ | 2 | 1 | 1 | 0 | 1/3 | 1/3 | – 2/3 | 0 | 1 | – 1 |
| $V_3$ | 3 | 0 | 1 | 0 | – 1/3 | 2/3 | – 1/3 | – 1 | 1 | 0 |
| $V_4$ | 4 | 0 | 1 | 1 | – 2/3 | 1/3 | 1/3 | – 1 | 0 | 1 |
| $V_5$ | 5 | 0 | 0 | 1 | – 1/3 | – 1/3 | 2/3 | 0 | – 1 | 1 |
| $V_6$ | 6 | 1 | 0 | 1 | 1/3 | – 2/3 | 1/3 | 1 | – 1 | 0 |
| $V_7$ | 0 (Origin) | 1 | 1 | 1 | 0 | 0 | 0 | 0 | 0 | 0 |

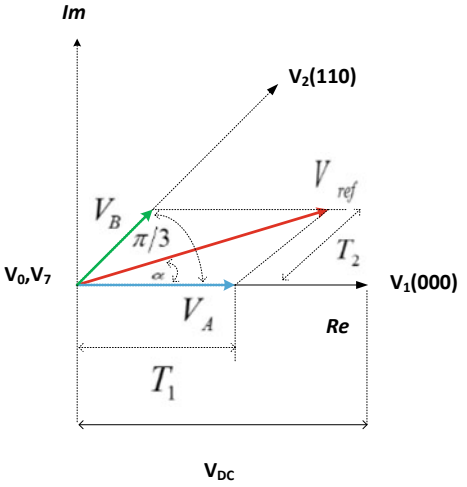


**Fig. 4** Calculation of $V_{\text{ref}}$, $T_1$, and $T_2$ in sector 1

2, $V_A = V_2$ and $V_B = V_3$. In the same way for every other sector, $V_{\text{ref}}$ shifts or moves left counterclockwise with a time lapse of $T_z$. $T_1$ is the time lapse for $V_A$, $T_2$ is the time lag for $V_B$, and $T_0$ is the time interval for $V_0$ and $V_7$. In sector 1 mathematical analysis, the duration of each $T$ time is determined by Eq. (8), Eq. (9), and Eq. (10):

$$T_1 = T_z.a.\frac{\sin\left(\frac{\pi}{3} - \alpha\right)}{\sin\left(\frac{\pi}{3}\right)} \tag{8}$$

$$T_2 = T_z.a.\frac{\sin(\alpha)}{\sin\left(\frac{\pi}{3}\right)} \tag{9}$$

$$T_z = T_1 + T_2 + T_0 \tag{10}$$

where $0 \leq \alpha \leq 60^0$; $T_z = \frac{1}{f_z}$; and $a = \frac{|\overline{V}_{\text{ref}}|}{\frac{2}{3}V_{\text{dc}}}$

Figure 4 explains each sector the value of is always in the interval $0 \leq \alpha \leq \frac{\pi}{3}$, in sector 1 $V_{\text{ref}}$ angle of $\alpha = 0^0$ is the same as $V_1$, for angle of $\alpha = \frac{\pi}{3}$ is parallel to $V_2$. In sector 2, $V_{\text{ref}}$ angle of $\alpha = 0^0$ is the same as $V_2$, for angle of $\alpha = \frac{\pi}{3}$ is parallel to $V_3$. And so on for calculations in other sectors [25] using Eq. (11) and Eq. (12).

Time duration in sector $n$

$$T_1 = \frac{\sqrt{3}T_z|\overline{V}_{ref}|}{V_{dc}}\left(sin\left(\frac{\pi}{3} - \alpha + \frac{n-1}{3}\pi\right)\right) \tag{11}$$

$$T_2 = \frac{\sqrt{3}T_2|\overline{V}_{\text{ref}}|}{V_{dc}}\left(\sin\left(\alpha - \frac{n-1}{3}\pi\right)\right) \tag{12}$$

where n = 1, 1 through 6 (that is, sectors 1 through 6, $0 \leq \alpha \leq 60^0$).

## 3 Method

The working method with the tool of Simulink MATLAB software through analyses parameters of each section in this paper such as voltage, gate pulse, stator currents, rotor currents, and much more positively impacted this study. It is the result of the design developed by the researcher (space vector modulation), which also produces various effects that can be used as a reference for other researchers due to the data analyzed.

Some of the parameters analyzed in this paper include the generation of reference voltages, the turn-on time of the inverter switch for each sector, gate pulses, stator currents, rotor currents, and the relationship between torque and DC motor speed. Figure 5 describes the research method used by building a path or wiring step from the designed system design. The working steps are as follows: The three-phase power source is a three-phase sine wave generator at a frequency of 50 Hz, and variable amplitude with a phase difference of 1200 for each wire. These three voltages are then transformed into a 2-coordinate system or abc—αβ which is called the park transformation. The reference voltage and the sector selection angle are used to determine the sector of the plane on the d-q coordinate axis where the stress vector is selected. There are six sectors in the d-q coordinate axis; each sector is 600. The next step is to determine the values of $T_z$, $T_1$, $T_2$, and $T_0$ using Eqs. 7, 8, 9, and 10 to get the timing pattern of the inverter ignition pulse. The inverter pulse generator is obtained by comparing the space vector modulator signal with a triangular carrier signal with a frequency of 4 kHz. The inverter is composed of 3 leg pairs of IGBT switches as Variable Speed Driver (VSD) activated by a pulse ignition pulse. A three-phase induction motor as a load is simulated with parameters 54 HP (4 kW), 400 V, 50 Hz, and 1430 rpm. The value of the DC link voltage on the inverter is 400 V. When the position vector is at $V_0$ and $V_7$ then no current flows in the load or $I_{\text{inv}} = 0$ A. All

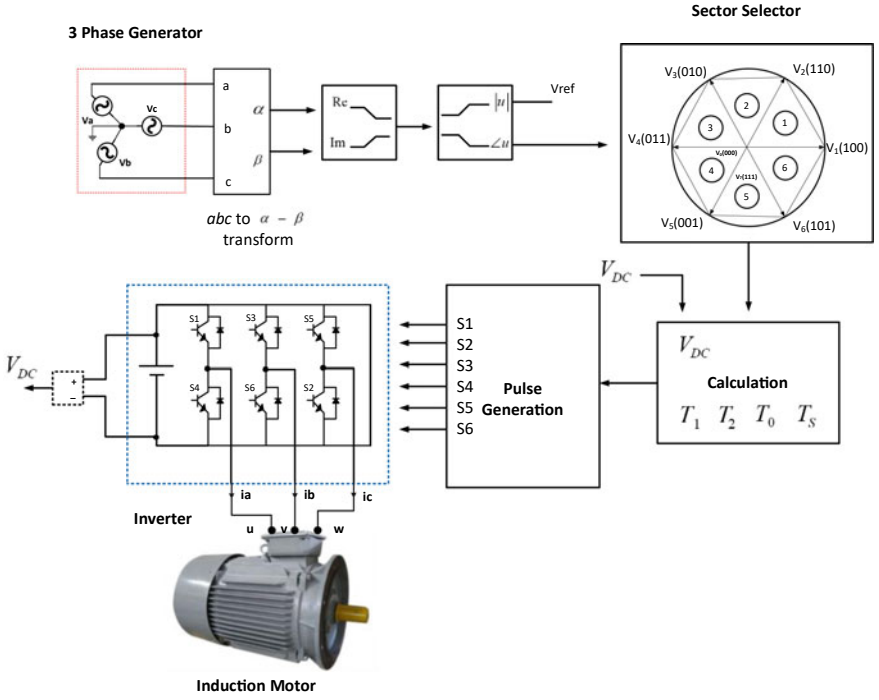


**Fig. 5** Design of a space vector modulation system for control of a three-phase induction motor

voltages in each sector are multiplied by $V_{dc}$. To change the magnitude of $abc$—$\alpha\beta$ or better known as park transformation, the three-phase source voltage is lowered to a level of 1 V, 50 Hz with different phase angles of $0^0$, $120^0$, and $120^0$. The system design in Fig. 5 is then modeled in Simulink MATLAB. The results of the modeling shown in Fig. 6 is a three-phase two-level inverter with a three-phase induction motor load.

## 4 Results and Discussion

Observations were made by running the modeling and then analyzing the simulated waves at the observed modeling image points. Using Eq. (1), the angle can be obtained in degrees in the form of a sawtooth wave with an amplitude of 3 $V_{(p-p)}$ (in the top figure). Figure 10 is the center of the angle in radians with an amplitude of 180 $V_{(p-p)}$, while the bottom picture is the value of $V_{beta}/V_{alpha}$ in the form of a sinusoidal wave with an amplitude of 1 $V_{(p-p)}$ with a phase difference of 900. Figure 7 is a graph of changes in load torque, electromagnetic torque, and induction motor speed with time. In the model built, the induction motor bears the load at different times. Load

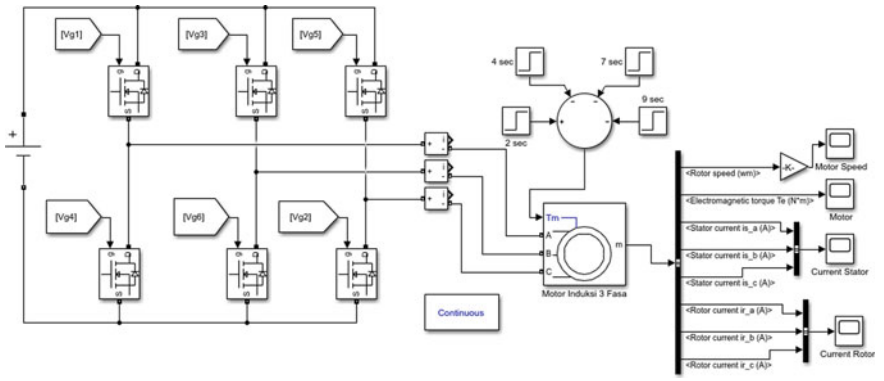


**Fig. 6** MOSFET two-level inverter as a three-phase induction motor drive

of three-phase induction motor with parameters 54 HP (4 kW), 400 V, 50 Hz, and 1430 rpm. So the relationship between motor torque and load torque can be analyzed as follows using Eq. (13):

$$T_a = T_L + T_{sh} \tag{13}$$

$T_a$ = torque (armature) or motor torque.

$T_{sh}$ = shaft torque = net power shaft torque.

$T_L$ = torque (loss).

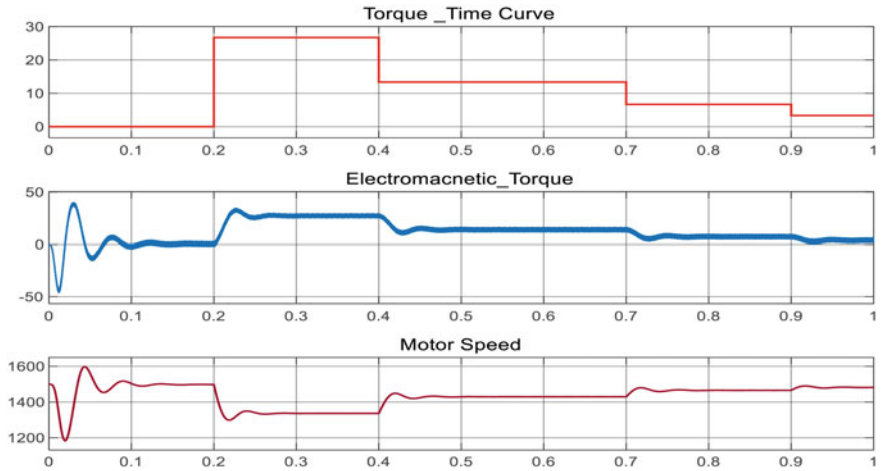


**Fig. 7** Load torque curve, electromagnetic torque, and induction motor speed

$T_{sh} = \frac{P_{out}}{\omega}$,
where $\omega = \frac{2\pi N}{60}$

$N$ = full load motor speed.

so $\omega = \frac{2\times3.14\times1430}{60} = 149.62$ rad/s.

$T_{\text{sh(max)}} = \frac{4000}{149.62}$

$T_{\text{sh(max)}} = 26.73$ Nm.

Table 2 shows that between 0 and 0.2 s the induction motor has not been loaded or when the motor is starting the load torque is at zero level and the speed of the induction motor is at a maximum of 1499 rpm. When the time is in the range 0.2 s–0.4 s, the motor is loaded and the maximum torque is 26.73 Nm; at this time, the speed of the induction motor drops and is at a minimum speed of 1334 rpm. The time is between 0.4 s and 0.7 s and between 0.7 s and 0.9 s the load is reduced so that the speed increases according to the decrease in load torque.

Figure 8 describes the change in stator current at the start, zero loads, maximum load and 1/2 maximum load, 1/4 maximum load torque, and 1/8 maximum load torque. It appears that at the start of the motor running, the motor draws a large current of about 50 $A_{(p-p)}$. After the motor rotates for a while, the current approaches zero when the time is between 0.1 s and 0.2 s at which time the motor has not been loaded and rises to a maximum when it is at 0.2 s < $t$ < 0.4 s maximum load torque. The current decreases over time between 0.4 s and 0.9 s following the decrease in load torque. The stator current pattern is in the form of a sinusoid with the same amplitude for each phase, and this magnitude affects the load torque.

Figure 9 shows the rotor current waveform when starting the motor, zero loads, 1/2 peak load, 1/4 peak load, and 1/8 peak loads. When starting the rotor current, a large current of about 45 $A_{(p-p)}$isdrawn, and then it drops to zero at zero loads. The rotor current reaches the maximum when full load torque is obtained when 0.2 s < $t$ < 0.4 s. Then the current slopes as the load torque decreases when 0.4 s < $t$ < 0.7 s and $t$ > 0.9 s. The current drawn by this rotor causes a change in the load torque. When the minimum rotor current, the load torque is close to zero, resulting in maximum motor speed.

Figure 10 is a simulation waveform of two voltage levels between three-phase lines $V_a$, $V_b$, $V_c$ and amplitude 400 $V_{(p-p)}$ at a frequency of 50 Hz with SVPWM control. This voltage has a THD which is still quite large. Reducing this level of

**Table 2** Net torque change of induction motor load against time

| Time (s) | Tsh (N.m) | Speed (rpm) |
|---|---|---|
| 0 < t < 0.2 | 0 | 1499 |
| 0.2 < t < 0.4 | $T_{\text{sh (max)}} = 26.72$ | 1435 |
| 0.4 < t < 0.7 | 1/2 $T_{\text{sh (max)}} = 13.36$ | 1468 |
| 0.7 < t < 0.9 | 1/4 $T_{\text{sh (max)}} = 6.68$ | 1484 |
| t > 0.9 | 1/8 $T_{\text{sh (max)}} = 3.34$ | 1492 |

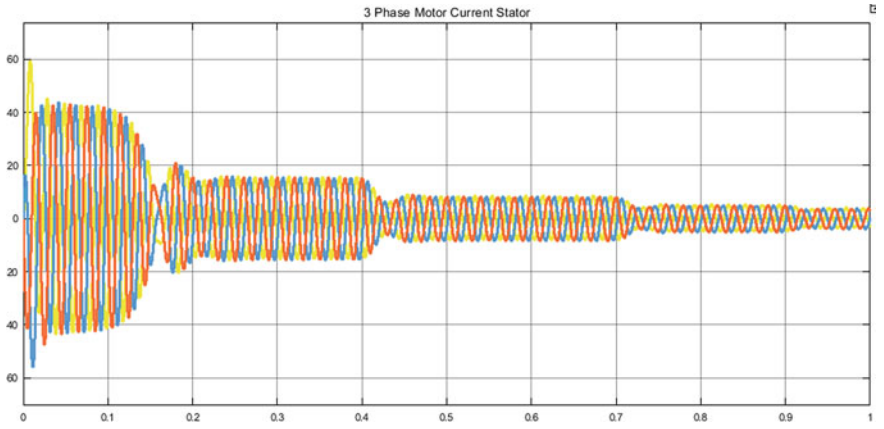


**Fig. 8** Stator current against changes in load torque at various times

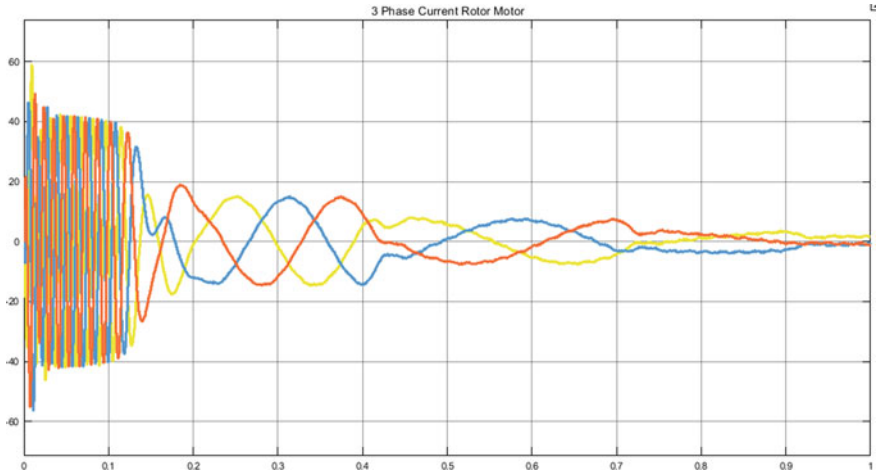


**Fig. 9** Rotor current at various load torque changes

harmonics can be overcome by increasing the number of levels at the output voltage by adding an inverter arranged in a cascade.

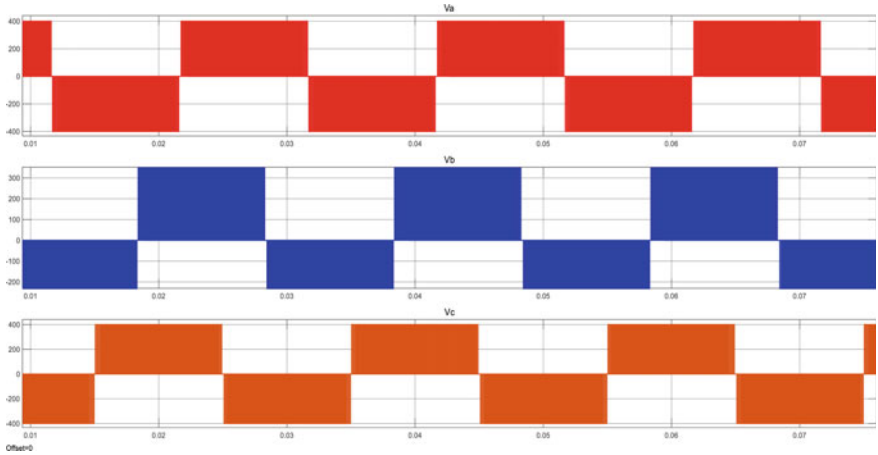


**Fig. 10** Inverter output voltage $V_a$, $V_b$, $V_c$ with SVPWM control

## 5 Conclusion

The Space Vector Pulse Width Modulation method is a pulse width modulation technique that is very effective in controlling the performance of asynchronous machines. Inverter trigger pulse generation is based on the performance component of the inverter switch which is divided into 6 sectors to get the reference voltage and sector angle values. The difference in the angle of the sector is $60^0$ for each sector. The duration and time pattern of the switching on of the inverter switch is the same, but the phase is different by $60^0$. The load torque of the induction motor is influenced by the rotor current which has ripples when the load changes at the start and when the motor experiences a load change. The two inverter output voltage levels still have a high Total Harmonics Distortion (THD) level, so a higher number of levels is needed so that the THD content can be reduced. This model is easy to implement into the actual circuit so that it can help researchers to make Variable Speed Drives (VSD) for induction motors with good control.

## References

1. Vashishtha S, Rekha KR (2021) Modified digital space vector pulse width modulation realization on low-cost FPGA platform with optimization for 3-phase voltage source inverter. Int J Electr Comput Eng 11, 3629–3638. https://doi.org/10.11591/ijece.v11i4.pp3629-3638
2. Strankowski P, Guzinski J, Morawiec M, Lewicki A, Wilczynski F (2020) Sensorless five-phase induction motor drive with third harmonic injection and inverter output filter. Bull Polish Acad Sci Tech Sci 68, 437–445. https://doi.org/10.24425/bpasts.2020.133369
3. Algamluoli AF, Abbas NH (2021) Speed controller design for three-phase induction motor based on dynamic adjustment grasshopper optimization algorithm. Int J Electr Comput Eng

11, 1143–1157. https://doi.org/10.11591/ijece.v11i2.pp1143-1157
4. Ali AJ, Khalaf LA, Ahmed AH (2021) Modeling and simulation of a 3-ϕ induction motor based on two types of WFA. Int J Electr Comput Eng 11, 1105–1113. https://doi.org/10.11591/ijece.v11i2.pp1105-1113
5. Al-Yoonus MA, Al-Deen Alyozbaky OS (2021) Detection of internal and external faults of single-phase induction motor using current signature. Int J Electr Comput Eng. 11, 2830–2841. https://doi.org/10.11591/ijece.v11i4.pp2830-2841
6. Benbouhenni H (2019) A comparison study between fuzzy PWM and SVM inverter in NSMC control of stator active and reactive power control of a DFIG based wind turbine systems. Int J Appl Power Eng. 8, 78 https://doi.org/10.11591/ijape.v8.i1.pp78-92
7. Wróbel KT, Szabat K, Serkies P (2019) Long-horizon model predictive control of induction motor drive. Arch Electr Eng 68, 579–593. https://doi.org/10.24425/aee.2019.129343
8. Kiani B, Mozafari B, Soleymani S, Mohammadnezhad Shourkaei H (2021) Predictive torque control of induction motor drive with reduction of torque and flux ripple. Bull Polish Acad Sci Tech Sci 69, 1–13. https://doi.org/10.24425/bpasts.2021.137727
9. Zahraoui Y, Akherraz M, Fahassa C, Elbadaoui S (2020) Induction motor harmonic reduction using space vector modulation algorithm. Bull Electr Eng Informatics 9, 452–465. https://doi.org/10.11591/eei.v9i2.1682
10. Youcef M, Djilali T, Moreau S, Said H, Bachir D (2021) Dsp improvement of a vector speed induction motor control with a rst and adaptive fuzzy controller. Bull Electr Eng Informatics 10, 1232–1244. https://doi.org/10.11591/eei.v10i3.1798
11. Kadum AA (2020) New adaptive hysteresis band width control for direct torque control of induction machine drives. Int J Power Electron Drive Syst 11, 1908–1917. https://doi.org/10.11591/ijpeds.v11.i4.pp1908-1917
12. Fang J, Wang G, Li R, Liu S, Wang S (2021) Improved virtual space vector modulation for neutral point voltage oscillation and common-mode voltage reduction in neutral point clamped three-level inverter. Arch Electr Eng 70, 203–218. https://doi.org/10.24425/aee.2021.136062.
13. Elkholi OA, Enany MA, Abdo AF, Eid M (2020) Novel approach for svpwm of two-level inverter fed induction motor drive Int J Power Electron Drive Syst 11, 1750–1758. https://doi.org/10.11591/ijpeds.v11.i4.pp1750-1758
14. Kadum AA (2020) PWM control techniques for three phase three level inverter drives. Telkomnika (Telecommunication Comput Electron Control 18, 519–529. https://doi.org/10.12928/TELKOMNIKA.V18I1.12440
15. Shashibhushan S, Sonoli S (2019) Starting torque and torque ripple reduction using SVPWM based vector control of induction motor with nine-level cascaded multilevel inverter fed with solar PV power. Int J Power Electron Drive Syst 10, 1123. https://doi.org/10.11591/ijpeds.v10.i2.pp1123-1132
16. Hasoun M, Afia A, El Khafallah M, Benkirane, K (2020) A pwm strategy for dual three-phase pmsm using 12-sector vector space decomposition applied on electric ship propulsion. Int J Power Electron Drive Syst 11, 1701–1710. https://doi.org/10.11591/ijpeds.v11.i4.pp1701-1710
17. Tomasov V, Usoltsev A, Zolov P, Gribanov P (2017) The effect of space vector modulation algorithm on characteristics of three-phase voltage inverter for drives of optical telescopes. Bull Polish Acad Sci Tech Sci 65:629–637. https://doi.org/10.1515/bpasts-2017-0068
18. Bouziane M, Abdelkader M (2019) Direct space vector modulation for matrix converter fed dual star induction machine and neuro-fuzzy speed controller. Bull Electr Eng Informatics. 8, 818–828. https://doi.org/10.11591/eei.v8i3.1560
19. Shults TE, Husev O, Blaabjerg F, Roncero-Clemente C, Romero-Cadaval E, Vinnikov D (2019) Novel space vector pulsewidth modulation strategies for single-phase three-level NPC impedance-source inverters. IEEE Trans Power Electron 34:4820–4830. https://doi.org/10.1109/TPEL.2018.2859194
20. Vashishtha S, Rekha KR (2018) A survey: Space vector PWM (SVPWM) in 3φ voltage source inverter (VSI). Int J Electr Comput Eng. 8, 11–18. https://doi.org/10.11591/ijece.v8i1.pp11-18

21. Mahsahirun SN, Idris NRN, Yusof ZM, Sutikno T (2020) Fundamental elements of constant volt/hertz induction motor drives based on dspace ds1104 controller. Int J Power Electron Drive Syst 11, 1670–1685. https://doi.org/10.11591/ijpeds.v11.i4.pp1670-1685
22. Selvakumar K, Palanisamy R, Stalin AR, Gopi P, Ponselvin P, Saravanan K (2019) Simulation of 3-phase matrix converter using space vector modulation. Int J Electr Comput Eng 9, 909. https://doi.org/10.11591/ijece.v9i2.pp909-916
23. Sharma A, Anandh N, Gao S (2020) Modulation index effect on inverter based induction motor drive. Int J Power Electron Drive Syst 11, 1785–1798. https://doi.org/10.11591/ijpeds.v11.i4.pp1785-1798.
24. Pongiannan CB, Yusuff RK, Tariq A, Maddileti M, Tharwinkumar TT (2019) A simple switching on-time calculation revision in multilevel inverter-space vector modulation to achieving extended voltage boundary operation. Int J Power Electron Drive Syst 10, 653. https://doi.org/10.11591/ijpeds.v10.i2.pp653-661
25. Porwal A, Baria K, Deshpande A (2014) Modeling and simulation of svpwm based application. 3:140–148